UNCLASSIFIED

AD 273 402

Reproduced
by the

ARMED SERVICES TECHNICAL INFORMATION AGENCY
ARLINGTON HALL STATION
ARLINGTON 12, VIRGINIA

UNCLASSIFIED

NOTICE: When government or other drawings, specifications or other data are used for any purpose other than in connection with a definitely related government procurement operation, the U. S. Government thereby incurs no responsibility, nor any obligation whatsoever; and the fact that the Government may have formulated, furnished, or in any way supplied the said drawings, specifications, or other data is not to be regarded by implication or otherwise as in any manner licensing the holder or any other person or corporation, or conveying any rights or permission to manufacture, use or sell any patented invention that may in any way be related thereto.

62-74

273 402

JOURNAL OF APPLIED MECHANICS AND THEORETICAL PHYSICS (SELECTED ARTICLES)

By

Various Authors

UNEDITED ROUGH DRAFT TRANSLATION

JOURNAL OF APPLIED MECHANICS AND THEORETICAL PHYSICS
(SELECTED ARTICLES)

BY: Various Authors

English Pages: 37

SOURCE: Zhurnal Prikladnoy Mekhaniki i Tekhnicheskoy Fiziki, No. 4, 1961, pp. 82-93, 94-101.

THIS TRANSLATION IS A RENDITION OF THE ORIGINAL FOREIGN TEXT WITHOUT ANY ANALYTICAL OR EDITORIAL COMMENT. STATEMENTS OR THEORIES ADVOCATED OR IMPLIED ARE THOSE OF THE SOURCE AND DO NOT NECESSARILY REFLECT THE POSITION OR OPINION OF THE FOREIGN TECHNOLOGY DIVISION.

PREPARED BY:

TRANSLATION SERVICES BRANCH
FOREIGN TECHNOLOGY DIVISION
WP-AFB, OHIO.

TABLE OF CONTENTS

THE MOVEMENT OF A FREE SURFACE OF HOMOGENEOUS GROUND DURING AN UNDERGROUND EXPLOSION

N. I. Onis'ko and Ye. I. Shemyakin

The problem on the propagation of seismic waves in a semi-unbounded elastic medium from an unstationary, spherically symmetric source is examined. This problem was set up in connection with the study of wave processes formed in the ground during underground explosions. The main attention is devoted to the construction of theoretical oscillograms of the displacement of points on a free surface of a medium. It is assumed that the wave source is described by a function chosen on the basis of experimental data on camouflaged explosions.

§1.1. Let a signal source be set in a homogeneous isotropic elastic medium having Lame's constants λ and μ and density ρ on some sphere of radius R_o with center at the point o (Fig. 1). In the problem of wave propagation during underground explosions, the signal may be described by the velocity of a particle $u_R = u_R(t)$ during its movement along the radius from the point o or by the normal stress $\sigma_R = \sigma_R(t)$.

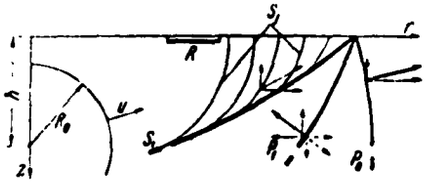

Fig. 1. For stating the problem.

Let us examine the propagation of a signal $u_R(t)$. Let us assume that at $t < 0$ the medium is at rest, and the signal is inserted at $t = 0$.

In a problem with central symmetry, for an elastic medium the movement of a particle along the radius w may be represented in the form

$$w(R, t) = \frac{\partial}{\partial R}\left[\frac{\Phi(\xi)}{R}\right], \qquad \xi = t - \frac{R - R_0}{v_p}, \qquad v_p = \frac{\lambda + 2\mu}{\rho} \tag{1.1}$$

Here $\Phi(\xi)$ and v_p are the potential and velocity of the distribution of longitudinal waves

$$\frac{\partial w}{\partial t} = u_R(t) \quad \text{at} \quad R = R_0 \tag{1.2}$$

where $u_R(t) = u_0 f(t)$ is a present function, u_0 the constant dimension of the velocity, $f(t)$ some continuous function, and $f(0) = 0$.

The equation for $\Phi(\xi)$ follows from (1.2). Its solution at zero starting data $\Phi(0) = \Phi'(0) = 0$ is determined by the function

$$\frac{\Phi(\xi)}{R} = -\frac{u_0 R_0^2}{R}\int_0^{\xi} f(\xi - \tau)\left[1 - \exp\left(-\frac{\tau v_p}{R_0}\right)\right] d\tau \tag{1.3}$$

The displacement $w(r, t)$ is determined by differentiation with respect to R, and the velocity of the particle $u_R(R, t)$ is determined by additional differentiation with respect to t.

In the future it will be useful to represent formula (1.3) in the form

$$\frac{\Phi(\xi)}{R} = -u_0 R_0^2 \int_0^{\xi} f_1(t)\left[\frac{1}{2\pi i}\int_{\sigma-i\infty}^{\sigma+i\infty} \frac{e^{s(\xi-\tau)}}{s^2}\, ds\right] d\tau$$

$$f_1(\tau) = \frac{R_0}{2\pi i}\int_{\sigma_1-i\infty}^{\sigma_1+i\infty} \frac{F(\mu)}{R_0\mu + v_p}\, e^{\mu\tau} d\mu, \qquad F(\mu) = \int_0^{\infty} f(t)\, e^{-\mu t}\, dt \tag{1.4}$$

Here, in the contour intergals $\sigma > 0$ and $\sigma_1 > 0$.

The following may be concluded on the basis of (1.4). The solution of the problem on the propagation of a signal in elastic media may be examined first of all for some elementary signal $\Phi_0(\xi)$, and then, using (1.4), one can move to the actual change of the signal in time. This corresponds to the replacement of the signal assigned to the sphere $R = R_0$ by a signal from a spatially concentrated source.

In the future the role of $\Phi_0(\xi)$ will be played by the potentials

$$\Phi_\delta(\xi) = \frac{u_0 R_0^2}{R}\frac{1}{2\pi i}\int_{\sigma-i\infty}^{\sigma+i\infty}\frac{e^{s\xi}}{s}ds,\quad \Phi_\varepsilon(\xi) = -\frac{u_0 R_0^2}{R}\frac{1}{2\pi i}\int_{\sigma-i\infty}^{\sigma+i\infty}\frac{e^{s\xi}}{s^2}ds \tag{1.5}$$

describing the change in the velocity of the particles in time for a concentrated source of type $\delta(t)$ and the change of the point source in time as $\varepsilon(t)$ respectively. In these formulas $\delta(t)$ is Dirac's function, and $\varepsilon(t)$ is a step function

$$\varepsilon(t) = \begin{matrix} 0 & (t<0) \\ 1 & (t\geqslant 0) \end{matrix},\quad \delta(t) = \frac{d\varepsilon(t)}{dt}$$

Several transformations are necessary in order to use Formula (1.5) in the cylindrical coordinate system (r,θ,z). As a result, the first formula of (1.5) takes the form

$$\Phi_\delta(\xi) = -u_0 R_0^2\int_0^\infty kJ_0(kr)\left\{\frac{1}{2\pi i}\int_{(l)}\frac{\exp\left[st'(h-z)\sqrt{a^2s^2+k^2}\right]}{s\sqrt{a^2s^2+k^2}}ds\right\}dk \tag{1.6}$$

Here $\underline{h}$ is the ordinate of the center of the source, $\underline{z}$ the ordinate of the point of observation, and $(\underline{l})$ the contour:

$$\xi = t' - a\sqrt{r^2+(h-z)^2},\quad t' = t + aR_0,\quad a = \frac{1}{v_p}\quad (\mathrm{Re}\, s = \sigma > 0).$$

Formula (1.6) describes the disturbances emanating from the source in the direction of the negative semiaxis $\underline{z}$.

In conclusion to Section 1, let us introduce formulas analogous to (1.4) for a signal of the second type. On a sphere of radius $R=R_0$ the normal stress $\sigma_R(t) = -\sigma_0 g(t)$ is assigned, where σ_0 is the dimensionality constant of the stress, $g(t)$ is some continuous function, and $g(0) = 0$.

In this case, instead of (1.3), we have the formula [1]

$$\frac{\Phi(\xi)}{R} = -\frac{\sigma_0 R_0}{\rho R}\int_0^{\xi} g(\xi-\tau)\, e^{-n\tau}\frac{\sin m\tau}{m}\,d\tau \qquad \left(n=\frac{2\mu a}{\rho R_0},\ m=n\sqrt{\frac{\lambda+\mu}{\mu}}\right) \tag{1.7}$$

and instead of (1.4)

$$\frac{\Phi(\xi)}{R} = -\frac{\sigma_0 R_0}{\rho}\int_0^{\xi} g_1(\tau)\left[\frac{1}{2\pi i}\int_{\sigma-i\infty}^{\sigma+i\infty}\frac{e^{s(\xi-\tau)}}{sR}\,ds\right]d\tau \tag{1.8}$$

where

$$g_1(\tau) = \frac{1}{2\pi i}\int_{\sigma-i\infty}^{\sigma+i\infty}\frac{sG(s)\,e^{s\tau}}{m^2+(s+n)^2}\,ds, \qquad G(s) = \int_0^{\infty} g(t)\,e^{-st}\,dt$$

The expressions for the potentials of elementary signals in spherical and cylindrical coordinates preserve the previous form.

Let us derive formulas for calculating the main normal stresses $\sigma_R(R, t)$ and $\sigma_\varphi(R, t)$, at an arbitrary point in the medium, which correspond to the source $\sigma_R(t)$

$$\frac{\sigma_R(R,t)}{\rho} = \frac{\Phi^*(\xi)}{R} + 4\frac{v_s^2}{v_p}\frac{\Phi_1(\xi)}{R^2} + 4v_s^2\frac{\Phi(\xi)}{R^3}, \qquad v_s^2 = \frac{\mu}{\rho}$$

$$\frac{\sigma_\varphi(R,t)}{\rho} = \left(1-\frac{v_s^2}{v_p^2}\right)\frac{\Phi^*(\xi)}{R} - 2\frac{v_s^2}{v_p}\frac{\Phi'(\xi)}{R^2} - 2v_s^2\frac{\Phi(\xi)}{R^3} \tag{1.9}$$

Formulas (1.9) were derived using (1.1), (1.7) and Hooke's law and describe the complex change in the stresses with distance as compared with the change in pressure in an analogous problem for a fluid. As follows from (1.9), the presence of second and third terms in these formulas is fully explained by the resistance of the medium to dis-

placement ($\mu \neq 0$). If $\mu = 0$, i.e., $v_s = 0$ (the propagation rate of transverse waves v_s vanishes at $\mu \neq 0$), then from (1.9) follows the solution of the problem for a fluid

$$\sigma_R(R, t) = \sigma_\varphi(R, t) = \frac{\rho\Phi''(\xi)}{R} \tag{1.10}$$

The first terms in (1.9) determine the asymptotic behavior of the stresses at $R \to \infty$. If the concept of the length of a nonstationary wave $\lambda = v_p T$ is introduced, where T is some characteristic time of the signal, then the first terms in (1.9) will describe the behavior of the stresses in time with high accuracy at distances $R \gg \lambda$. We are mainly interested studying the disturbance fields at distances comparable to the wave length. In this case we cannot be limited to asymptotic formulas and should turn to accurate formulas.

2. Let us examine the problem for an elastic half-space $z \geq 0$, if within it at the point $z = h$ an elementary signal is sent which describes a longitudinal-wave field having a potential of the type (1.5) for a signal of the type $u_R(t)$.

The solution can be set up either by the method of V. I. Smirnov and S. L. Sobolev [2] or by the method of partial division of the variables [3].

As is known, when a wave describable by a longitudinal (or transverse) potential $\Phi_0(\xi)$ strikes a free surface $z = 0$; waves describable by longitudinal $\varphi_1(r,z,t)$ and transverse $\psi_1(r,z,t)$ potentials are reflected the surface. The potentials of the reflected field may be represented by the following expressions:

$$\varphi_1(r, z, t) = \int_0^\infty R_1(z, t, k) J_0(kr)\, dk$$

$$\psi_1(r, z, t) = \int_0^\infty S_1(z, t, k) J_1(kr)\, dk$$

$$R_1(z,\ t,\ k) = \frac{1}{2\pi i}\int_{\sigma-i\infty}^{\sigma+i\infty} X_1(k,\ s)\, e^{st-z\alpha_1}ds,$$

$$S_1(z,\ t,\ k) = \frac{1}{2\pi i}\int_{\sigma-i\infty}^{\sigma+i\infty} Y_1(k,\ s)\, e^{st-z\beta_1}ds \tag{1.11}$$

Here

$$X_1(k,\ s) = -\frac{T}{R}X_0(k,\ s), \qquad Y_1(k,\ s) = -\frac{4k\alpha_1 g}{R}X_0(k,\ s)$$
$$\alpha_1 = \sqrt{a^2s^2+k^2}, \quad \beta_1 = \sqrt{b^2s^2+k^2}, \quad g = 2k^2+b^2s^2$$
$$b = \frac{1}{v_s}, \quad R = g^2-4k^2\alpha_1\beta_1, \quad T = g^2+4k^2\alpha_1\beta_1$$

In this R_1 and S_1 are represented by Mellinovskiy contour integrals, and $X_0(k, s)$ should be taken according to (1.6) in the form

$$X_5(k,\ s) = -u_0R_0^2\frac{k}{s^2\alpha_1}e^{-h\alpha_1} \tag{1.12}$$

or according to (1.5) in the form

$$X_6(k,\ s) = -u_0R_0^2\frac{k}{s^2\alpha_1}e^{-h\alpha_1} \tag{1.13}$$

On the basis of Functions (1.11), (1.12) and 1.13), formulas determining the reflected displacement field for a point source of the type (1.12) in the half-space $z \geq 0$ may be reduced to the form

$$w_r(r,\ z,\ t) = u_0R_0^2\int_0^\infty kJ_1(kr)\left\{\frac{1}{2\pi i}\int_{(l)}\left[\frac{\delta^2+4\alpha\beta}{\delta^2-4\alpha\beta}e^{-k(h+z)\alpha} - \right.\right.$$
$$\left.\left. - \frac{4\alpha\beta\delta}{\delta^2-4\alpha\beta}e^{-kz\beta-kz\alpha}\right]\exp\frac{k\zeta t}{b}\frac{d\zeta}{\zeta\alpha}\right\}dk$$
$$w_z(r,\ z,\ t) = -u_0R_0^2\int_0^\infty kJ_0(kr)\left\{\frac{1}{2\pi i}\int_{(l)}\left[\frac{\delta^2-4\alpha\beta}{\delta^2+4\alpha\beta}e^{-k(h+z)\alpha} - \right.\right.$$
$$\left.\left. - \frac{4\delta}{\delta^2-4\alpha\beta}e^{-kz\beta-kz\alpha}\right]\exp\frac{k\zeta t}{b}\frac{d\zeta}{\zeta\alpha}\right\}dk \tag{1.14}$$

Here

$$\alpha = \sqrt{1+\gamma^2\zeta^2}, \quad \gamma = \frac{v_s}{v_p}, \quad \beta = \sqrt{1+\zeta^2}, \quad \delta = 2+\zeta^2$$

and (1) is Mellinovskiy's contour $\mathrm{Re}\zeta=\sigma > 0$; $\arg \alpha = \arg \beta = 0$ at $\zeta > 0$.

The displacement field described by Formulas (1.14) is caused by movements in a longitudinal wave from an elementary source (1.12)

$$w_{r\delta} = \frac{u_0 R_0^2}{R} \frac{r}{R} \left[a\delta (t - aR) + \frac{\delta (t - aR)}{R} \right]$$
$$w_{z\delta} = -\frac{u_0 R_0^2}{R} \frac{h - z}{R} \left[a\delta (t - aR) + \frac{\delta (t - aR)}{R} \right] \tag{1.15}$$

The entire field of displacements (1.14) and (1.15), corresponding to source (1.12), will be studied in Section 3 and is subsidiary in this problem.

The main attention will be devoted to the study of the displacement field on the surface of an elastic medium in order to obtain accurate oscillograms of the motion of points on the surface for signal (1.13). In this Expressions $w_r(r, 0, t)$ and $w_z(r, 0, t)$, determined below, describe the total field of movement

$$w_{rz}(r, 0, t) = 2A \int_0^\infty J_1(kr) \left\{ \frac{1}{2\pi i} \int_{(l)} \frac{\beta}{\delta^2 - 4\alpha\beta} \exp\left[k \left(\zeta \frac{t}{b} - h\alpha \right) \right] d\zeta \right\} dk$$
$$w_{zz}(r, 0, t) = -A \int_0^\infty J_0(kr) \left\{ \frac{1}{2\pi i} \int_{(l)} \frac{\delta}{\delta^2 - 4\alpha\beta} \exp\left[k \left(\zeta \frac{t}{b} - h\alpha \right) \right] d\zeta \right\} dk \tag{1.16}$$
$$(A = 2u_0 R_0^2)$$

In conclusion to Section 2, let us note that the solutions of (1.14) and (1.16) obtained by the method of partial division of the variables permits an elementary investigation of the asymptotic behavior of the components of the displacement field. This was demonstrated by the works of a Leningrad group under the direction of G.I. Petrashen'.

In this problem, the asymptotic study of the formulas obtained will be subsidiary to the qualitative study of the properties of the

wave field on the basis of Formulas (2.4) and (2.5).

In Section 3 we shall examine the qualitative wave pattern in an elastic half-space. Detailed investigations of the accurate solutions of problems on the dynamic theory of elasticity, carried out by a group of Leningrad dynamics specialists [3,4 and 1], allow, when explaining the qualitative wave pattern, the fundamental properties of the wave fields to be established quickly in concrete problems if solutions of the type (1.14) are set up.

These investigations were made using asymptotic methods for contour integrals (the method of stationary phase) with subsequent integration according to Fourier--Bessel and are intended, chiefly, for studying the field at long distances from the source ($R >> \lambda$). In this a single-valued correspondence is set up between the properties of the integrands of the contour integrals from (1.14) and the qualitative properties of the wave field [5].

3. Without repeating the cumbersome calculations of the principal terms in the asymptotic representations of the disturbances in the vicinity of the wave front, let us introduce the picture of the fronts of the wave field at some moment in time (Fig. 1.) and write the corresponding approximate formulas.

1°. In the vicinity of the front of a direct longitudinal wave P_0, the displacement field is described by Formulas (1.15) for the source (1.12).

If Formula (1.4) is taken into account and we move to a given change of the source in time, the main parts of the disturbances at $\sqrt{r^2 + (h - z)^2} >> \lambda$ will have the form

$$w_r \approx \frac{u_0 R_0^2}{v_p R} x f_1(\xi), \qquad w_z \approx -\frac{u_0 R_0^2}{v_p R} \sqrt{1 - x^2} f_1(\xi) \qquad (x = \sin \alpha) \tag{1.17}$$

where α is the angle of incidence of the wave P_0 to the boundary.

If (1.17) is examined along some plane z = 0, which passes through an unbounded elastic medium at a distance $\underline{h}$ from the center of the source, then w_r decrease as in an unbounded medium: R^{-1} at $R \to \infty$, and w_z will decrease as R^{-2}.

2°. In the vicinity of the front of a reflected longitudinal wave P_1, the main terms in the approximate asymptotic formulas have the form

$$x_{rp} \approx -\frac{u_0 R_0^2 x G_1(x)}{r_p \sqrt{r^2+(h-z)^2}} f_1(\xi_1), \qquad \xi_1 = t' - a\sqrt{r^2+(h+z)^2}$$

$$w_{zp} \approx -\frac{u_0 R_0^2 G_1(x)\sqrt{1-x^2}}{r_p \sqrt{r^2+(h-z)^2}} f_1(\xi_1) \tag{1.18}$$

Here

$$G_1 = \frac{(2\gamma^2x^2-1)^2 - 4\gamma^3x^2\sqrt{1+x^2}\sqrt{1-\gamma^2x^2}}{(2\gamma^2x^2-1)^2 + 4\gamma^3x^2\sqrt{1-x^2}\sqrt{1-\gamma^2x^2}}$$

describes the change in amplitude of the reflected wave as a function of the angle of reflection α. It is interesting to note that the entry sign of the reflected wave can change, as the graph of the function G_1 for $\gamma = 0.6$ attests (Fig. 2). In accordance with these graphs in Fig. 2, the arrow on the front of the wave P_1 indicates the direction of the motion of the particle when entering this wave.

Formulas (1.18) indicate the nature of the change of movement in time, as in the direct wave P_0.

3°. In the vicinity of the front of a transverse wave S_1, formed together with the reflected wave P_1, the corresponding approximate formulas have the form

$$w_{rs} \approx \frac{u_0 h_0^2 \sqrt{1-\gamma^2 x^2}}{v_p h^*} G_2(x) f_1(t - t_\psi)$$

$$w_{zs} \approx -\frac{u_0 h_0^2 \gamma x}{v_p h^*} G_2(x) f_1(t - t_\psi)$$

(1.19)

Here $G_2 = \frac{4\gamma x^2 \sqrt{1-x^2}(1-2\gamma^2 x^2)}{(2\gamma^2 x^2 - 1)^2 + 4\gamma^3 x^2 \sqrt{1-x^2}\sqrt{1-\gamma^2 x^2}}$, $R^* = x\left\{r \tan\alpha \left[h + \gamma z \left(\frac{1-x^2}{1-\gamma^2 x^2}\right)^{3/2}\right]^{-1}\right\}^{1/2}$

and t_f is the arrival time of the transverse wave at an observation point[1] with coordinates (r, z) such that $t_f = t_1 + t_2$, where t_1 is the running time of the wave P_0 to the boundary $z = 0$, and t_2 is the running time of the transverse reflected wave S_1. Let us recall the mechanism of the formation of the transverse wave S_1. At each point on the surface $z = 0$ at which the longitudinal wave P_0 arrived, compressions, and displacements, which are then propagated with different velocities V_p and V_s. Fig. 1 shows elementary waves S_j leaving a free

surface and going into the depths of space. The transverse wave S_1 will be the envelope of these waves, the equation of this envelope at some fixed moment $t = t_f$.

The function $G_2(x)$ for all x and γ will remain positive (Fig. 3), this attests to the fact that the entry signs of the transverse wave at the moment $t = t_f$ in the notations $w_r(r, z, t)$ and $w_z(r, z, t)$ at all distances r at fixed values of z and h are not changed: in entry of a transverse wave a particle is moved above and ahead of the source, moving along the tangent to the front of wave S_1 (Fig. 1).

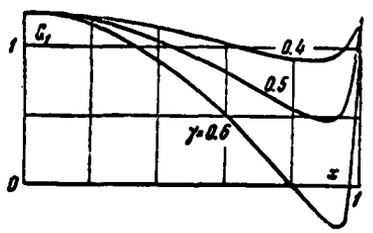

Fig. 2. Graphs of $G_1(x)$ for γ = =0.4--I, γ = 0.5--II [1] and γ = 0.6--III.

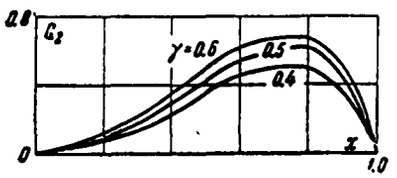

Fig. 3. Graphs of $G_2(x)$. Values of γ same as in Fig. 2.

As was noted above, for the problem at hand a correspondence is set up between the properties of the integrands of the contour integrals and the properties of the disturbance field in the solution of (1.14). In the Mellin integrals from (1.14) the integrands have simple poles at the points $\zeta = \pm i\vartheta (0 < \vartheta < 1)$ of the complex plane ζ. The residues at the points $\zeta = \pm i\vartheta$ and subsequent elementary integration with respect to k allows it to be established that the property of the

---

[1] The time t_f is determined by the formula

$$t_f = \frac{1}{v_p}\sqrt{(r-r_0)^2+h^2}+\frac{1}{v_s}\sqrt{r_0^2+z^2}$$

Here r_0 for fixed values of r, z, h is determined from Snell's law $\gamma \sin\alpha = \sin\beta$, where β is the angle of reflection of a transverse wave S_1.

disturbance field connected with this is none other than a surface wave of the Rayleigh type [4]. In Section 2 this disturbance was examined in more detail, by accurate formulas for the entire disturbance field. It should be noted that the principal part of this disturbance is propagated with a rate $v_R = \vartheta v_s < v_s$ and, therefore, all of this disturbance appears mainly during the observation times $t_R \approx r/v_R$ for given $r > h$ and $r > z$.

This observation was made by analogy with known results, but may be easily demonstrated by calculating the residues at the points $\zeta = \pm i\vartheta$ in (1.14), and by careful analysis of the properties of this wave in our problem. Fig. 1 shows this by a conventional symbol and the letter R is the surface wave.

Finally, let us introduce the approximate formulas for the components of the displacement field on the free surface of the medium. At points on the surface z = 0 these formulas describe the total field of movements $P_0 + P_1 + S_1$ and may be obtained either by asymptotic methods directly from (1.14) or by summation of the main parts of (1.15), (1.18) and (1.19)

$$w_r(r, 0, t) \approx \frac{4u_0 R_0^2 G_3(x)}{v_p \sqrt{r^2 + h^2}} f_1(\xi)$$
$$w_z(r, 0, t) \approx -\frac{2u_0 R_0^2 G_4(x)}{v_p \sqrt{r^2 + h^2}} f_1(\xi) \qquad (1.20)$$

Here ξ is according to (1.20); the functions

$$G_3 = \frac{1}{\Delta(x)} \gamma(x) \sqrt{1 - x^2} \sqrt{1 - \gamma^2 x^2}, \quad G_4 = \frac{1}{\Delta(x)} \sqrt{1 - x^2}(1 - 2\gamma^2 x^2)$$
$$\Delta(x) = (2\gamma^2 x^2 - 1)^2 + 4\gamma^3 x^2 \sqrt{1 - x^2} \sqrt{1 - \gamma^2 x^2}$$

As follows from (1.20), the components of the movement field decrease differently with distance, as is illustrated by the graphs in Figs. 4 and 5.

In connection with the graphs of $G_3(x)$ and $G_4(x)$, it should be noted that at $r >> \lambda$ the laws of amplitude reduction with distance for the displacement field and rate field are the same; it varies only as a curve.

These qualitative properties of wave disturbances allow the fundamental types of waves in a medium, their kinetic and dynamic features, to be shown. As usual, the wave propagation rates and arrival time of waves at a given point of observation pertain to the first. The asymptotic laws of the damping of amplitude, the comparative intensities of the manifestation of various waves, and their entry signs on a theoretical oscillogram refer to the second.

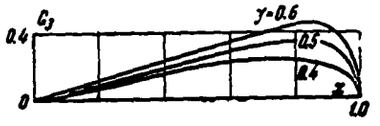

Fig. 3. Graphs of $G_3(x)$.

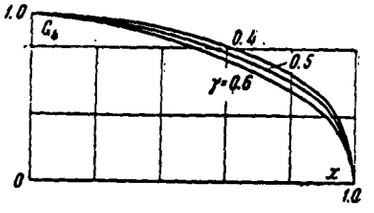

Fig. 4. Graphs of $G_4(x)$.

At the same time it is almost apparent that these formulas are hardly applicable for quantitative comparisons with experimental data, save for a medium which is very nearly elastic, and at distances $r >> \lambda$. In order to obtain more accurate descriptions of elastic wave disturbances in the vicinity of the fronts of volume waves it is necessary to either calculate the successive terms of the asymptotic expanstion or to calculate by accurate formulas.

§2.1 Accurate investigations of the displacement field may be carried out either by solutions obtained by the Smirnov--Sobolev method [2] or by formulas of type (1.14) or (1.16). Bearing in mind

the problem, let us limit ourselves below to the study of the displacement field on the surface z = 0 (1.16).

Ogurtsov and Petrashen' [4] have indicated a simple method reducing and formulas of the type (1.16) to real integrals. In this, in the contour integrals, the location of segments along the imaginary axis from the lower point of branching to infinity are chosen from (1.16) (symmetrical to the upper and lower points of branching to infinity), and the contour is deformed to the edges of the segments.

The subsequent rearrangement of the order of integration and integration with respect to $\underline{k}$ allow (1.16) to be represented in the form of the following simple expressions in the dimensionless variables ξ, η, t^*:

$$w_{r\varepsilon} = \frac{k}{t^*}[U_{r0} + U_{rR} + U_{r\lambda}], \quad k = \frac{u_0 R_0}{v_s}, \quad t^* = \frac{tv_p}{R_0}$$
$$w_{z\varepsilon} = \frac{k}{t^*}[U_{z0} + U_{zR} + U_{z\lambda}], \quad \xi = \frac{r}{tv_p}, \quad \eta = \frac{h}{tv_p} \tag{2.1}$$

Here

$$U_{r0} = \frac{\gamma}{1-\gamma^2}\frac{\xi}{(\xi^2+\eta^2)^{3/2}}, \quad U_{rR} = \frac{4\sqrt{1-\vartheta^2}}{\xi d_1\sqrt{\rho}}\left(\eta\sqrt{1-\gamma^2\vartheta^2}\sin\frac{\varphi}{2} + \frac{v_R}{v_p}\cos\frac{\varphi}{2}\right)$$
$$\rho = \sqrt{[\xi^2+\eta^2(1-\gamma^2\vartheta^2) - v_R^2a^2]^2 + 4v_R^2a^2\xi^2(1-\gamma^2\vartheta^2)}$$
$$\varphi = \arctan\left(\frac{2v_Ra\eta\sqrt{1-\gamma^2\vartheta^2}}{a^2v_R^2 - \xi^2 - \eta^2(1-\gamma^2\vartheta^2)} + \frac{\pi}{2}\right), \quad v_R = \vartheta v_s, \quad a = \frac{1}{v_p}$$
$$d_1 = 4\left(2 - \vartheta^2 - \gamma^2\frac{\sqrt{1-\vartheta^2}}{\sqrt{1-\gamma^2\vartheta^2}} - \frac{\sqrt{1-\gamma^2\vartheta^2}}{\sqrt{1-\vartheta^2}}\right)$$

and φ is the root of the equation

$$(2-\vartheta)^2 = 4\sqrt{1-\vartheta^2}\sqrt{1-\gamma^2\vartheta^2}$$
$$U_{z0} = -\frac{\gamma}{1-\gamma^2}\frac{\eta}{(\xi^2+\eta^2)^{3/2}}, \quad U_{zR} = \frac{2-\vartheta^2}{d_1\sqrt{\rho}}\sin\frac{\varphi}{2}$$

The items $U_{r\lambda}$ and $U_{z\lambda}$ are represented by the real integrals

$$U_{r\lambda} = -\frac{4}{\pi\xi}\int_1^{1/\gamma} \frac{(2-\lambda^2)^2\sqrt{\lambda^2-1}}{P(\lambda)}\left(\eta\sqrt{1-\gamma^2\lambda^2}\sin\frac{\varphi_1}{2}+\gamma\lambda\cos\frac{\varphi_1}{2}\right)\frac{\xi d\lambda}{\sqrt{\rho_1}}$$

$$U_{z\lambda} = -\frac{8}{\pi}\int_1^{1/\gamma} \frac{(2-\lambda^2)\sqrt{\lambda^2-1}\sqrt{1-\gamma^2\lambda^2}}{P(\lambda)}\sin\frac{\varphi_1}{2}\frac{d\lambda}{\sqrt{\rho_1}} \qquad (2.2)$$

Here

$$P(\lambda) = (2-\lambda^2)^4 + 16(\lambda^2-1)(1-\gamma^2\lambda^2),$$

and ρ_1 and φ_1 are obtained from ρ and φ by substitution of λ for ϑ.

These formulas make it possible to conduct accurate studies of the displacement field on the surface of an elastic medium. From physical considerations it is clear that the calculation should be made at $\xi^2 + \eta^2 \leq 1$. After calculating (2.1) and (2.2), transition to the source, which varies in time according to the law f(t), is accomplished using the formula

$$w(r, z, t) = \int_0^{t^*} f_2(t-\tau)\, w_\varepsilon(r, z, t)\, d\tau \qquad (2.3)$$

where

$$f_2(\tau) = f(\tau) - \int_0^{\tau} f(v)\exp(v-\tau)\, dv$$

Let us make two comments in connection with formulas (2.1), (2.2) and (2.3). The solution for the displacement field in the elastic problem can be written as a function of the dimensionless variables ξ, η, t^*. This means that for all elastic media having various parameters v_p, v_s, ρ, but having fixed γ, in the problem on may calculate the universal curves of $w_r(t^*)$ and $w_z(t^*)$ at a given point of observation. In this a scale in units of k is chosen for the ordinate and the dimensionless time t* is plotted along the abscissa. In this problem the notation of the velocity of particles on a sphere of

radius R_0 is chosen[1] as the signal f(t). If the signal parameters u_0 and R_0 are fixed, during transition from one elastic medium to another the scales of the displacements will vary in inverse proportion to the velocity of the transverse waves.

If (2.3) or (2.1) is differentiated with respect to time (moving to theoretical oscillograms for the velocity of particles on the surface of the ground), the scale factor for particle velocity may be established:

$$k_1 = \frac{u_0 R_0}{\gamma} \tag{2.4}$$

If it is assumed that u_0 and R_0 are fixed values for various elastic media, then it can be demonstrated that at equal dimensionless distances the amplitudes of the particle velocities vary in inverse proportion to γ. The ratio $\gamma = v_s/v_p$ for most real ground [6] varies little: γ = 0.4 to 0.6, therefore, the corresponding amplitudes of the particle velocity will differ little.

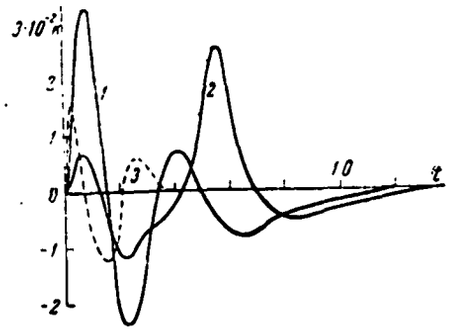

Fig. 6

[1] R_0 should be taken as that distance from the charge at which the effect of the free surface upon the recording of f(t) is not substantial.

These remarks also determine the direction of the numerical investigations whose results are given below.

2. Let us take as a basis a medium having parameters v_p = 4500 m/sec and $\gamma = 1/\sqrt{3}$. As follows from Formula (2.1) and (2.2), the density of the medium evidently does not enter the formula for the displacements anywhere, so that v_p and γ fully describe the required mechanical properties of a medium having parameters close to that of rock of medium hardness.

Let us take the distance 30 R_3 for R_0, where R_3 is the radius of the charge; the depths of the charges are 20 R_3 and 40 R_3. For signal f(t), used in the calculation and having a duration $t^* \approx 4$, some nominal wavelength may be taken as equal to $\lambda = R_0 t^* \approx 4\ R_0 = 120\ R_3$.

This also determined the range of calculated dimensionless distances r = 60 to 240 R_3.

Let us examine first of all the theoretical oscillograms of displacements at a distance r = 120 R_3 for h = 20 R_3 (Fig. 6). The theoretical oscillograms of r = 120 R_3, h = 20 R_3 are continuous lines: 1--the horizontal component of motion, and 2--the vertical. In the same scale along the abscissa Fig. 6 shows the form of the signal f(t) (curve 3) in an arbitrary vertical scale (the time of reading the signal is shifted to the entry time of the wave P_0). In comparison with the signal f(t) the shape of the curves of $w_r(t^*)$ and $w_z(t^*)$ is more complex: the total duration of the signal was increased; the ratio of the amplitudes of successive peaks and troughs is different on various components; and instead of a simple radial motion in the wave P_0 in an unbounded medium the motion of a surface particle has polarization (Fig. 7). The study of the trajectory of a particle jointly with accurate oscillograms and the qualitative

pattern of §1, Section 3 allows it to be concluded that various waves take part in the complex motion of a surface particle: $P_0 + P_1 + S_1 + +(S_j)$ and R. If we turn to Fig. 1, where the wave fronts P_0, P_1, S_1 and the waves S_j and R are shown schematically, we can interpret the complex motion of the surface in Fig. 7 as follows. The beginning of the motion of a surface point--above and ahead of the epicenter--corresponds mainly to motion in the longitudinal wave P_0 and includes reflection effects: P_1, S_1. This motion is accomplished elliptic orbit with clockwise particle rotation. After the transitional stage with particle motion below and behind, and then above and ahead, particle motion begins in a counterclockwise elliptic orbit. This motion is identified with the wave R, and the transitional stage is identified with motion in transverse waves S_j whose envelope is also the transverse wave S_1.

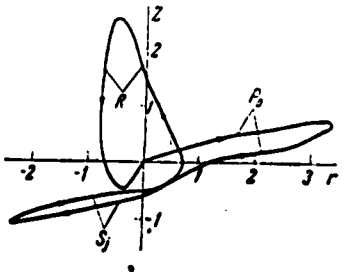

Fig. 7. Trajectory of a particle of the surface of a medium, according to data in Fig. 6.

In conclusion to the qualitative analysis, it should be noted that separation of complex motion into individual waves is conditional and contains the following concept. Separated sections of theoretical oscillograms and trajectories are identified with individual waves on the basis of kinematic and dynamic properties according to the preeminent manifestation of the properties of the individual waves in

These sections. Generally speaking it is impossible to deny the appearance of longitudinal waves in section S_j and of transverse waves S_j in section R, but this manifestation of additional disturbances is weaker than the fundamental motions, the indices of which are appropriate to the section.

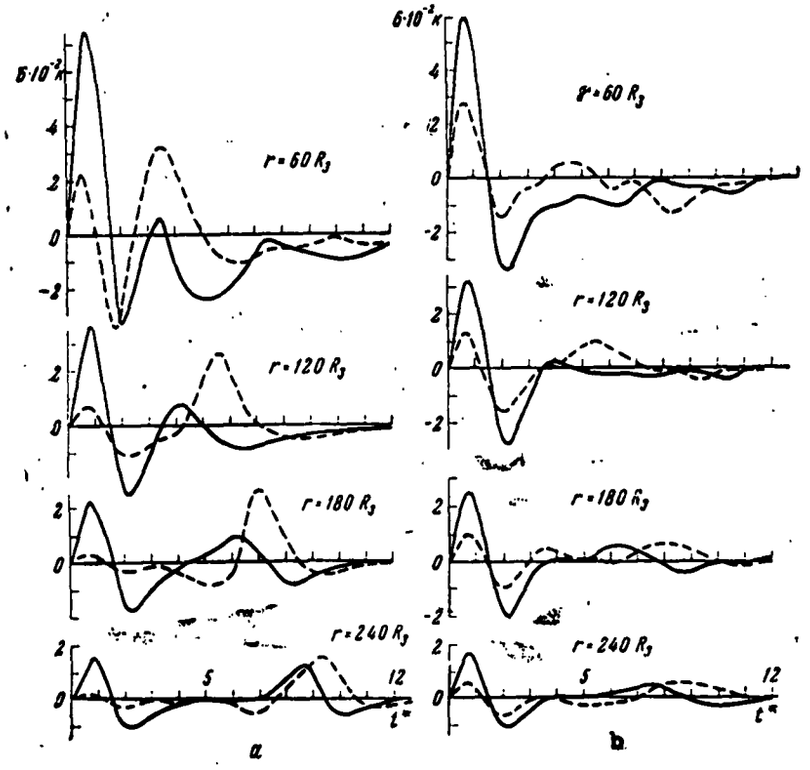

Fig. 8a. Theoretical oscillograms for h = 20 $R_з$, the arrival time of wave P_0 at a given point is plotted along the abcissa in units of t*. Symbols of components are the same as in Fig. 6.

Fig. 8b. Theoretical oscillograms for h = 40 $R_з$.

Figs. 8a and 8b show combined theoretical oscillograms of the motion of a surface for these same parameters of the medium, for the distances and depths indicated there.

Even a cursory examination of the oscillograms in Fig. 8a ($h = 20\ R_з$) makes it possible to clearly distinguish two fundamental groups in the motion of points on the surface $z = 0$, which, in accordance with the qualitative analysis, are denoted by the indices P and R (P_0, P_1 and S_1 in the first group, and S_j and naturally R in the second). These groups are propagated at various rates: the first at v_p and the second at v_R. The maximum amplitudes in these groups decrease with an increase in r according to various laws: while at close distances ~ 60 $R_з$ the first group predominates in amplitude, then, starting from the distance ~ 120 $R_з$, the second group starts to predominate. At this same distance motion in the transitional section possesses a comparatively insignificant amplitude, manifesting itself mainly in the phase of retrogressive motion in the first group and in sections of growth of the second.

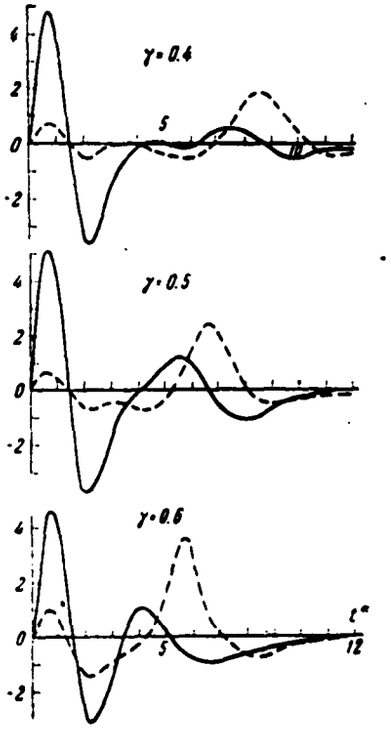

Fig. 9. Theoretical oscillograms for r = 120 $R_з$, h = 20 $R_з$ and γ = 0.4, 0.5 and 0.6.

On the basis of the calculations, in spite of small number of points with respect to the distances, it can be shown that at close distances the maximum displacements in the first group are decreased with distance not slower than r^{-1}, while at the end of the calculated range transition is projected to the law (1.15): displacements decrease more rapidly than r^{-1}, but more slowly than r^{-2}. If a graph is constructed of the damping of the maximum amplitides of displacements or velocities according to 1.15) for a chosen network of distances and depth $h = 20\ R_3$, it is possible to approximate this dependence by an exponential of the form Ar^{-n}, where n = 1.6 to 1.7. This law is the same for both displacements and particle velocities. It should be noted that it becomes applicable earlier (at closer distances) for describing particle velocities. In the calculated range in the second group the displacements decrease more slowly than r^{-1}, but more rapidly than $r^{-1/2}$ and more closely to the latter law, which is asymptotic for the surface wave R. This comparative characteristic allows change of the carrier of maximum amplitide to be indicated in general motion with an increase in distance from the epicenter. In this the first group may be traced more clearly on the horizontal component (first maximum and first minimum), and the second wave group on the vertical component, at the end of recording.

Fig. 8b shows theoretical oscillograms for a charge depth h = = 40 R_3. A comparison of the oscillograms in Figs. 8a and 8b indicates that the group which is identified by a surface wave has considerably less amplitide in Fig. 8b, although some decrease in amplitude is noted in the first wave-group. At $h = 40\ R_3$ change of the carrier of maximum amplitude does not take place in the entire calculated range of distances. From a comparison of the damping of maximum

amplitudes in the first and second groups it can be proved that this change at $h = 40\ R_3$ also takes place, but at greater distances than at a source depth $h = 20\ R_3$.

In conclusion let us note that the fundamental properties of the wave pattern do not in essence depend upon the concrete function $f(t)$ in the calculations. The only important fact here is that $f(t)$ determines a certain wavelength λ, which is the characteristic dimension in the problem, and this, in turn, determines the range of distances $r \approx \lambda$ under study.

3. Let us examine the change in the wave pattern occurring with a change in the value of γ. The parameter $v_p = 4500$ m/sec is fixed. Change in γ in this case denotes a change in the propagation rate of transverse and surface waves: when γ varies from 0.6 to 0.4, the value v_s varies from 2700 m/sec to 1800 m/sec. As follows from the theoretical oscillograms (Fig. 9), the second group lags behind the first more as γ decreases. In this it is possible to outline ($\gamma = 0.5$) and clearly separate ($\gamma = 0.4$) the intermediate maximum in motion in the transitional section, which corresponds to the second maximum of the signal $f(t)$. All fundamental properties of the wave pattern noted in Section 2 are preserved when γ varies. The maximum amplitudes of displacements when γ varies from 0.6 to 0.4 differ negligibly from the general law of dependence indicated by the scale factor $k = u_0R_0/v_s$. This follows from the graphs in Fig. 9, where all curves are constructed in a single vertical scale $k = u_0R_0/1800$.

In conclusion let us point out that this qualitative analysis of the wave pattern of the motion of a free surface of an elastic medium should be supplemented by an analysis of the changes in spectrum and energy in elastic motion of the boundary. These problems are separate due to their complexity and size and will be the subject of

special discussions.

The Author thanks K. Ye. Gubkin, V. N. Rodionov and A. N. Romashov for valuable discussion of the results of work in the preparation of this article.

REFERENCES

1. K. I. Ogurtsov, N. I. Yermilova and I. N. Uspenskiy. Some Quantitative Studies on Wave Propagation, Sb. Voprocy dinamicheskoy teorii rasprostraneniya seismicheskikh voln. Ch. I, Gostoptekhizdat, 1957.

2. V. I. Smirnov and S. L. Sobolev. A New Method for Studying Elastic in Space in the Presence of Axial Symmetry, Tr. Seysm. in-ta AN SSSR, No. 29, 1933.

3. G. I. Petrashen'. General Quantitative Theory of Reflected and Head Waves, Sb. Voprocy dinamicheskoy teorii rasprostraneniya seismicheskikh voln, Ch. I, Gostoptekhizdat, 1957.

4. K. I. Ogurtsov and G. I. Petrashen'. Dynamics Problems for Elastic Half-Space, Uch. zad. LGU, ser. matem., Vol. 21, No. 35, 1950.

5. K. I. Markov and Ye. I. Shemyakin. The Propagation of Disturbances in a Fluid Layer in Contact with Elastic Half-Space, PMM, Vol. XXI, Issue 1, 1957.

6. A. P. Volin and A. G. Rudakov. Seismic Explorations by Transverse Waves, Prikladnaya geofizika, Gostoptekhizdat, Issue, 15, 1956.

Submitted May 9, 1961

DEMOLITION OF A SOLID BY AN EXPLOSION

V. V. Adushkin and A. P. Sukhotin

In this work we will examine the demolition of a Plexiglas block by the explosion of a spherical charge inside it. The motion occurring during the explosion has a spherical symmetry which facilitates observation and interpretation of the experimental results. We will note that to study the qualitative picture of demolition the selection of the solid being demolished by the explosion is not important.

The experimental data cited in this work made it possible to elucidate certain aspects of the demolition of a solid by an explosion. A general picture of destruction is obtained and the time characteristics of the process are evaluated. It is shown that during demolition (both in the inside zone and with the shatter) it is necessary to distinguish two aspects: the conception of cracks and their development. It turned out that the space-time characteristics of the demolition process substantially depend on the behavior of the material in the immediate vicinity of the explosion point. The presence of a plastic zone near the discharge is equivalent to an increase in the dimensions of the source radiating an elastic wave.

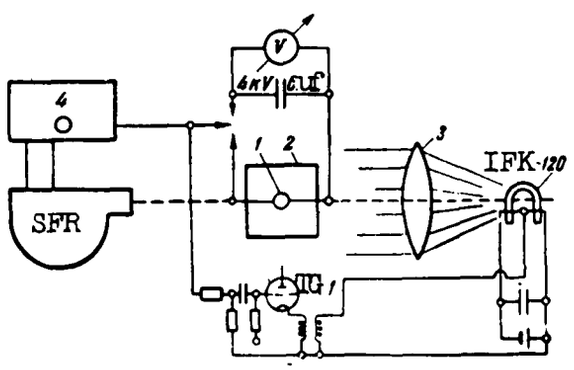

Fig. 1. Diagram of Experiments

Description of experiments. Plexiglas(poly(methyl)methacrylate) was selected as the solid to be demolished by explosion. We will cite the physical characteristics of Plexiglas taken from the handbook [1]:

Density	1.16--1.20 g/cm^3
Sound velocity	2800--3000 m/sec
Heat capacity	0.35--0.40 cal/g · deg
Thermal conductivity	(1--10)·10^{-4} cal/cm·sec·deg
Tensile strength	~1000 kg/cm^2

The blocks were cemented together from Plexiglas sheets 30-50 mm thick with V-31-F9 glue or with a 3% solution of Plexiglas in dichloroethane. Several experiments were made with monolithic blocks. We will cite the dimensions of the blocks which were tested:

h =	60	70	80	100	100	100	140	140 mm
d =	100	70	100	100	100	150	140	150 mm
l =	100	90	100	100	250	150	140	180 mm

In the center of the block we placed a charge of pressed PETN weighing 0.8 g with a radius of r_o = 5 mm, or a cast charge of TNT-RDX 50/50 weighing 24 g with a radius of r_o = 15 mm. In the experiments with monolithic blocks, the charge was placed in a hole which was closed by a threaded Plexiglas stopper.

The development of the explosion and demolition of the block was photographed in the passage of light by means of a high-speed camera (SFR), which in addition to continuous time scanning permitted us to obtain a series of frames with a frequency of up to 2 million frames per second. Figure 1 shows the diagram for carrying out the experiments. Block 2 was set so that the surface of the splice was parallel to the light rays coming from the pulse lamp (IFK-120) through condenser lens

3. Detonation of charge 1 of the explosive was done by a high-voltage pulse obtained by discharge of condenser KBG-P ($C = 6\ \mu f$) charged to a voltage of 4 kv. Breakdown of the discharge gap in the detonation circuit was initiated by an electrical pulse supplied from control panel 4 (SFR). The instant of its delivery was coordinated with the position of the scanning mirror. This pulse switched on the booster lamp.

Results of the experiments. Figure 2 shows typical film frames of the demolition of a 100 x 100 mm block. Figures 3 and 4 show the continuous time-scanning of this process in blocks of different size (W denotes the distance from the center of the charge to the free surface). The wavefront and demolition zone are distinctly seen in the photographs. The general picture of the development of the basic phenomena during explosion of a PETN charge weighing 0.8 g in a Plexiglas block is shown in r-t coordinates in Fig. 5. Line I represents the track of the compression wavefront which is reflected from the free surface as a tension wave (line 2). The contour of region 3 shows the expansion of the charge chamber in time. Its development ceases in approximately 6 μ sec when the radius reaches the value $2r_0$. Starting from distance $3r_0$, about 6 μsec after the passage of the compression wavefront there is a new region in which the material is demolished, region 4. Line 4 on the graph shows the development of its dimensions in time. We see from the graph in Fig. 5 that in a block 100 mm thick ($20r_0$) the effect of the free surface (line 2) on the development of region 4 is absent at least during 24 μ sec.

Compression wave. The graph in Fig. 5 and the photographs show that the velocity of the compression wavefront varied in the range of distances to $(5\text{-}6)r_0$. The sample graph of the dependence of the

velocity of the front on the distance, which was obtained by a graphic differentiation of line 1, is shown in Fig. 6. The dashed line in the graph marks the value of the velocity of the longitudinal acoustic waves in the Plexiglas. We see from the graph that in the range from $1r_0$ to $(5\text{-}6)r_0$, the velocity of the compression wavefront varies from 5000-6000 m/sec to 2900 m/sec. The velocity of the front of the reflected wave (line 2 in Fig. 5) is somewhat slower than the velocity of the longitudinal acoustic waves and is less than 2600-2700 m/sec.

In some cases we see parallel to line 1 still another line (Fig. 7) whose origin is unexplained.

The magnitudes of the mass velocities in the compression wave can be estimated by the initial velocities of the movement of the free surface V_0, assuming that the velocity doubles with reflection. The initial velocities of the motion of the free surface at the instant of reflection of the compression wave were measured within about 10%. We will give the values of the mass velocities $U = V_0/2$ meters per second, as well as estimates of the radial stresses in the wavefront calculated by the formula $\sigma_{rr} = \rho_0 cU$:

$r/r_0 =$	5	6.8	7.4	10	
$U =$	100	75	55	30	м/sec
$\sigma_{rr} =$	3500	2600	1900	1050	kg/cм²

If we assume that at the interface with the charge the pressure in the wave equals 10^5 kg/cm^2, we can write approximately the law of attenuation of the maximum pressure in the compression wave with distance as

$$P \approx \frac{10^5}{(r/r_0)^2} \qquad (1)$$

Demolition of block. An examination of the pieces of the smashed block permitted us to refine certain details of the picture seen on the film frames. In all experiments with Plexiglas blocks, regardless of their dimensions, we observed the following typical picture of demolition. The Plexiglas in a range of distances from $1r_0$ to $3r_0$ has no apparent destruction, remaining transparent. In the vicinity of the charge there takes place a noticeable heating of the material ($\Delta t \approx 10°C$). As the evaluations showed it is impossible to explain the rise in temperature as the result of heat conduction. It is necessary, apparently, to assume that the material is heated due to shock compression and plastic deformation behind the wavefront. At distances of $(3\text{-}4)r_0$ we observed a spherical zone consisting of a large amount of fine, radially oriented cracks. The number of these cracks per unit surface decreases with distance. The orientation of the cracks attests to the fact that they developed as the result of the action of azimuthal tensile stresses.

It is interesting to note that the destruction occurring during reflection of a compression wave from the free surface (shatter) has exactly the same character. The resemblance of the form of the cracks in the shattered and central zones confirm that tensile stresses cause radial cracks in the range $(3\text{-}4)r_0$. We already noted (graph in Fig. 5, range 4) that the radial cracks in range $(3\text{-}4)r_0$ develop about 6 μsec after the passage of the compression wavefront. This means that azimuthal tensile stresses are absent in the compression wave front. They occur later as a result of the radial displacement of the material in the spherically spreading compression wave. Figure 8 shows the dependence of the velocity of the front of radial cracks on the distance which was obtained by a graphic differentiation of

curve 4 on the graph in Fig. 5. It follows from the graph in Fig. 8 that the front of the radial cracks after its development, at a distance of $3r_0$ has a velocity of about 2000 m/sec, which decreases to 1000 m/sec at a distance of $4r_0$. The magnitude of the velocity in this region is probably determined by the propagation of a certain phase of asimuthal tensile stresses and not by the velocity proper of the development of cracks. This is particularly indicated by the fact that the fracture zone consists of fine, separate cracks not connected together in the direction of propagation.

When $r > 4r_0$ we observe a change in the character of destruction; only individual cracks develop farther, forming a wavy type of fracture. Their development takes place with a velocity decreasing from 1000 m/sec to 500 m/sec at a distance of $(5\text{-}6)r_0$. With a farther propagation, the velocity of the cracks does not change. Apparently in the range exceeding $4r_0$ the tensile stresses in the wave attenuate so much that they become insufficient for generating new cracks.

The time role of the effect of the explosion products compressed in the cavity can be qualitatively exposed from a comparison with the experiment where the explosion of a charge occurred in a hole on the free surface of a plate of Plexiglas 50 mm thick ($10r_0$). The result of the experiment is plotted on the graph in Fig. 5, where curve 4_2 shows the development in time of the zone of radial cracks, region 4. The picture of the development of an explosion in this case was obtained just as in the case of an explosion inside the block. A substantial difference is that the single radial cracks cease growing already at a distance of $(4\text{-}5)r_0$. This can be explained by the fact that in the case of an explosion on the surface, the explosion products have the opportunity to spread out freely in the atmosphere as a result of which the stresses in the material are reduced.

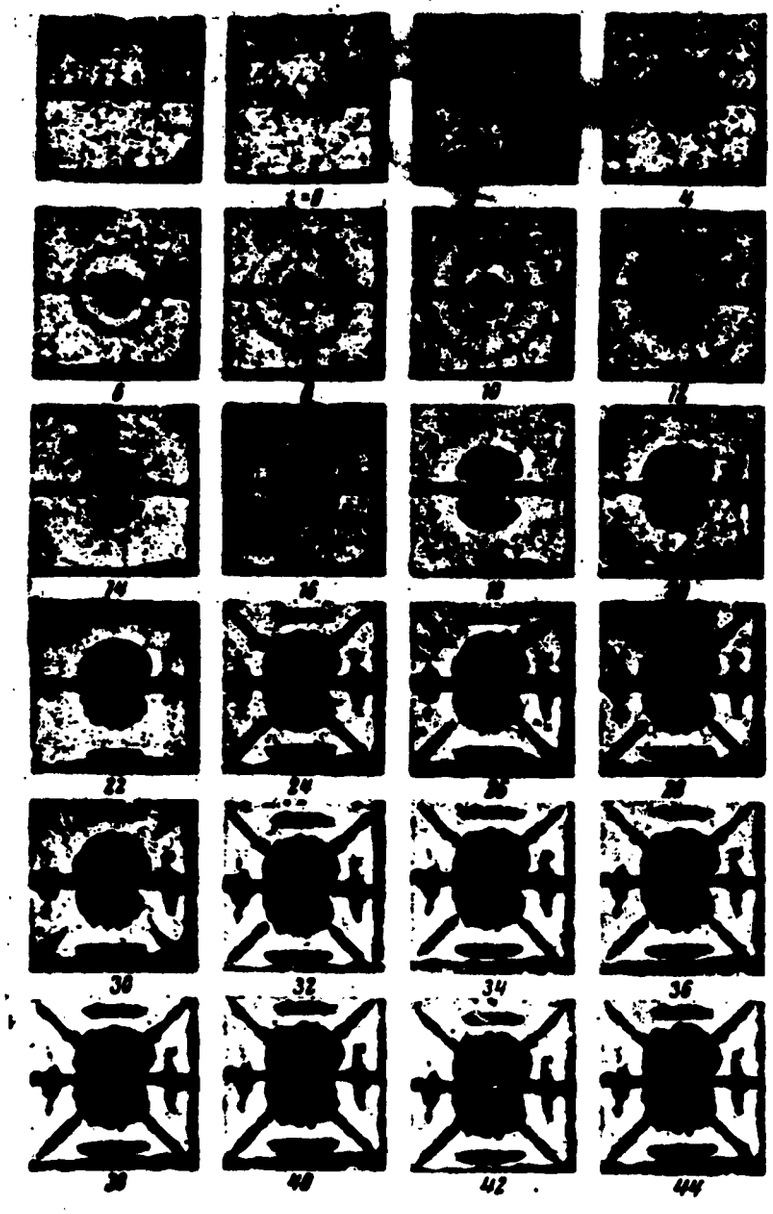

Fig. 2. Photographs of the development of the explosion of a PETN charge, C = 0.8 g, in glued block of Plexiglas. The time passing from the instant of explosion is shown under the frames in microseconds.

Fig. 3. Explosion of TNT-RDX 50/50, C = 24 g, in Plexiglas block ($2W = 10r_o$)

Fig. 4. Explosion of PETN charge, C = 0.8 g, in Plexiglas block ($2W = 20r_o$).

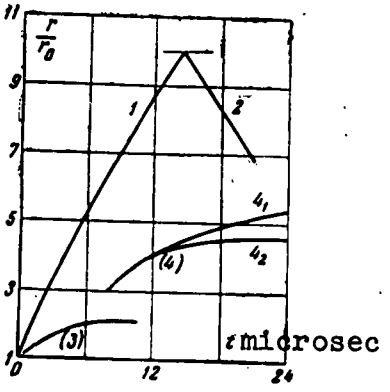

Fig. 5. r-t diagram of the development of the explosion in a block with thickness $2W = 20r_o$.

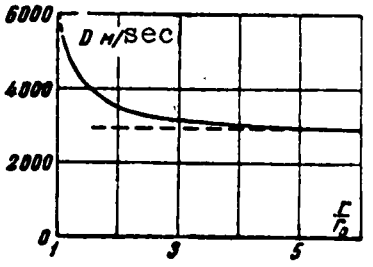

Fig. 6. Velocity of compression wavefront vs. distance.

Fig. 7. Explosion of PETN charge, C = 0.8 g, in Plexiglas block.

74

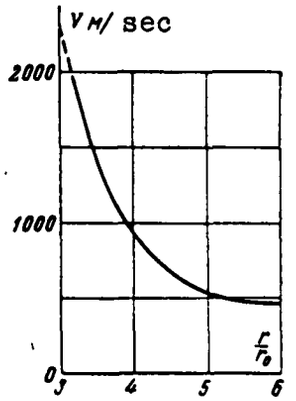

Fig. 8. Propagation velocity of the zone of radial cracks vs. distance.

It is interesting to note the effect of gluing on the picture of demolition. The film frames in Fig. 2 refer to a block glued by dichloroethane. It is apparent that gluing disrupts the properties of the Plexiglas, forming relieving surfaces. The experiments with blocks glued by V-31-F9 glue show that the semispherical regions of shattering are close together and, finally, the results of the experiment in the monolithic block attest to the fact that if the properties of the material are the same in all directions, the zone of destruction is a spherical surface. Figure 9 shows the film frames of this experiment with a 120 x 120 mm block.

Expansion of the discharge chamber. The development of a spherical dark spot, a cavity, (Fig. 2) is observed in the center of the block at the explosion site after the flash. Region 3 represents the cavity on the graph in Fig. 5. The dependence of the radius of the cavity r_k on time is shown in Fig. 10. The corresponding dependences for a gas bubble in water and a cavity in sand are shown on the same graph for comparison.

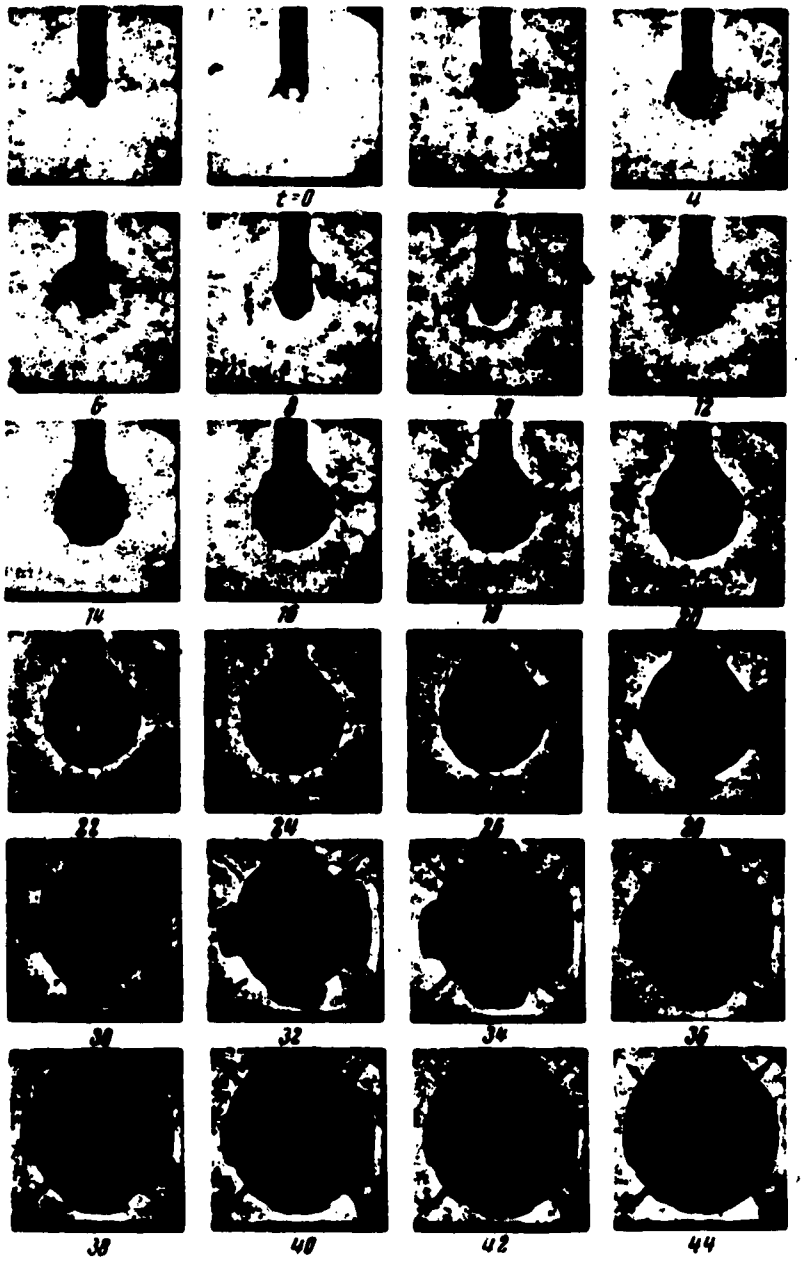

Fig. 9. Photographs of the development of an explosion of a PETN charge, C = 0.8 g, in a monolithic Plexiglas block. The time occurring from the instant of explosion in microseconds is indicated under the frames.

14

It is interesting that for the indicated media approximately the same law of motion was obtained in the initial expansion section

$$\frac{r_k}{r_0} = A\left(\frac{t}{c^{1/3}}\right)^{0.4} \qquad (2)$$

In the case of Plexiglas the maximum redius of the cavity based on the photographs reaches a magnitude of $2r_0$.

The measurements of the radius of the cavity where the explosive had been, based on the fragments of the blocks, show that the cavity radius increases on the average by only 20% (an expansion of the cavity to $1.2r_0$). A special test showed that optical effects here are excluded. At first glance such a contradictory behavior of the cavity can, apparently, be explained by the experimentally known capacity of Plexiglas for large reversible deformations during heating. Under the effect of the compression waves and pressure of the explosion products, the heated Plexiglas is expanded to the size shown in the photographs. The destruction of the block releases the compressed explosion products. This results in the elastic forces of the material compressing the cavity to a size of $1.2r_0$.

Shattering. Destruction in the vicinity of the free surface of the block (shatter) is caused by tensile stress which arises during the reflection of a wave from the free surface. Destruction of this type, which is observed in the present experiments, occurred practically at the front of the reflection wave. An examination of the fragments after the experiment showed that the shatter crack in the Plexiglas block is not a single continuous crack but is a certain zone of destroyed material 3-5 mm thick consisting of numerous small cracks in the form of lenticles or scales (0.5-3.0 mm in size). The shatter cracks are oriented parallel to the front of the reflection wave and only as a result of their development form an interface. When the

reserve of kinetic energy is sufficient in the piece intended for separation, the individual cracks of the boundary of the shatter zone grow, reach the free surface, and the small shatter plate flies off.

The noted type of shatter destruction and the fact that the shatter cracks which appeared are developed in time compels us to re-examine the frequently used assumption of the instantaneous destruction of material. It is necessary, apparently, to estimate carefully the time of destruction in each specific case. In the assumption of instantaneous destruction the head portion of the wave pulse is completely cut off by a crack. A certain delay in the formation of a shatter crack caused by its development can result in the head part of the wave curve in the stress-time coordinates changing its form in the region where the shatter cracks are developing. This in turn inevitably entails a change in the character of shatter destruction as a whole.

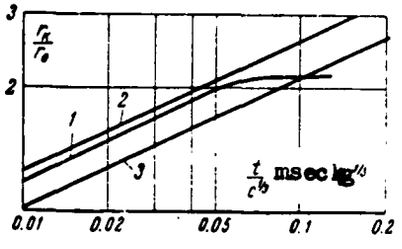

Fig. 10. Dependence of the radius of the cavity on time: 1) Plexiglas, A = 270; 2) water, A = 290; 3) sand, A = = 230.

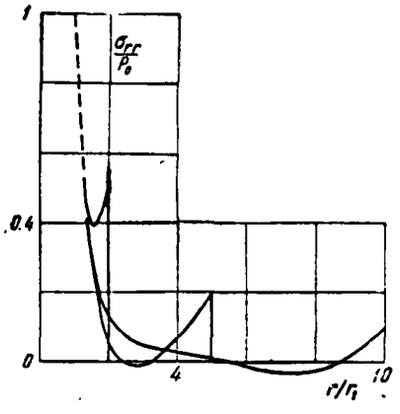

Fig. 11. Distribution of the radial components of the stresses behind the wavefront.

The Applicability of an Elastic Model of a Medium When Analyzing an Explosion in a Solid. Let us consider the simplest problem. In an elastic unbounded space with a Poisson ratio $\sigma = 1/3$ in a cavity

with radius r_1 at the instant of time t = 0 there instantaneously arises a pressure P_0 which then remains constant. Figures 11 and 12 show the results of the calculation in the form of a dependence

$$\sigma_{rr}/p_0 = f_1(r/r_1),\ \sigma_{00}/p_0 = f_2(r/r_1)$$

at different instants of time, where σ_{rr} is the stress in a radial direction, and σ_{00} is the stress in the azimuthal direction.

Let us compare the length of the positive phase of the compression wave λ_+, estimated by the thickness of the shattered plate δ, with the calculated value (Fig. 11). In the experiment with the block with the size $2W = 20r_0$ (r_0 = 5 mm) the thickness of the shatters plate was 10 mm. In this case the wave length $\lambda_+ - 2\delta = 20$ mm, which corresponds to $4r_0$.

It follows from the solution of the problem that for this case $r = 10\ r_0$, the value $\lambda_+ = 1.3r_0 = 6.5$ mm, i.e., in the experiment λ_+ is considerably greater than should have been in an elastic medium.

An examination of the graph in Fig. 12 shows that large tensile stresses σ_{00} are observed only in the neighboring zone at distances of $(1.5\text{-}2)r_1$. Beyond the limits of this zone σ_{00} sharply drops. The experiment shows, however, that the central zone of demolition has a size up to $(3.5\text{-}4)r_0$. Thus a comparison of the experimental data and of the results of the calculation with respect to the elastic model attest to the fact that this model cannot be used for describing the behavior of a material in the entire range of distances.

The difference between the experiment and the calculation, as well as the character of the observable destruction of the material proclaim that in the neighboring zone the material behaves explicitly inelastically. Thus, in the range of about $2.5r_0$ we observe a substantial heating of the material which indicates the presence in this zone of in-

elastic deformations. As distance from the charge increases the stresses in the wave drop and we can expect that with a certain distance $r = r_*$ the elastic model of the medium will apparently be justified to some extent. We will try to coordinate the qualitative picture, having selected as an appropriate sample a radius of the source of elastic oscillation r_1. If we select as r_1 the radius of the plastic region $2.5r_0$, then we will obtain a satisfactory agreement of the value of the shatter plate and the calculated wavelength and also of the radius of the formation of nuclei of radial cracks and of the zone of strong azimuthal stresses. We can assume that the plastic flow of material, which is observable during explosion, leads to an increase in the effective radius of the source in an elastic model.

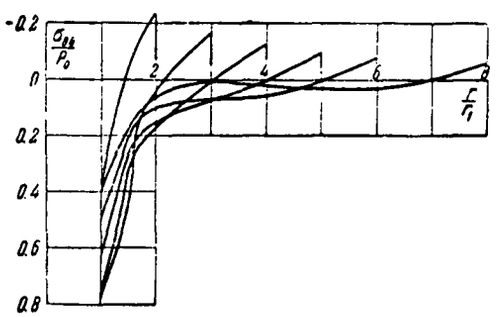

Fig. 12. Distribution of azimuthal components of stress behind the wave front.

Submitted June 9, 1961

REFERENCES

1. Handbook of Chemistry and Physics. 37th Edition, 1955--1956. Chemical Rubber Publishing Co.

DISTRIBUTION LIST

DEPARTMENT OF DEFENSE	Nr. Copies
HEADQUARTERS USAF	
AFCIN-3D2	1
OTHER AGENCIES	
CIA	1
NSA	2
AID	2
OTS	2
AEC	2
PWS	1
PGE	1
RAND	1

MAJOR AIR COMMANDS	Nr. Copies
AFSC	
SCFTR	1
ARO	1
ASTIA	10
TD-Bla	3
ASD (DCF)	1
AFSWC (SWY)	1